# MERS-CoV and H5N1 influenza virus antagonize antigen presentation by altering the epigenetic landscape

Vineet D. Menachery[a,b,1], Alexandra Schäfer[b,1], Kristin E. Burnum-Johnson[c], Hugh D. Mitchell[c], Amie J. Eisfeld[d], Kevin B. Walters[d,2], Carrie D. Nicora[c], Samuel O. Purvine[c], Cameron P. Casey[c], Matthew E. Monroe[c], Karl K. Weitz[c], Kelly G. Stratton[c], Bobbie-Jo M. Webb-Robertson[c], Lisa E. Gralinski[b], Thomas O. Metz[c], Richard D. Smith[c], Katrina M. Waters[c], Amy C. Sims[b,3], Yoshihiro Kawaoka[d,e,f,3,4], and Ralph S. Baric[b,g,3,4]

[a]Department of Microbiology and Immunology, University of Texas Medical Branch, Galveston, TX 77555; [b]Department of Epidemiology, University of North Carolina at Chapel Hill, Chapel Hill, NC 27599; [c]Biological Sciences Division, Pacific Northwest National Laboratory, Richland, WA 99354; [d]Influenza Research Institute, Department of Pathobiological Sciences, School of Veterinary Medicine, University of Wisconsin–Madison, Madison, WI 53706; [e]Division of Virology, Department of Microbiology and Immunology, Institute of Medical Science, University of Tokyo, Tokyo 113-8654, Japan; [f]International Research Center for Infectious Diseases, Institute of Medical Science, University of Tokyo, Tokyo 113-8654, Japan; and [g]Microbiology and Immunology, University of North Carolina at Chapel Hill, Chapel Hill, NC 27599

Contributed by Yoshihiro Kawaoka, December 14, 2017 (sent for review May 15, 2017; reviewed by Cornelia Bergmann, Brenda G. Hogue, and Vincent J. Munster)

**Convergent evolution dictates that diverse groups of viruses will target both similar and distinct host pathways to manipulate the immune response and improve infection. In this study, we sought to leverage this uneven viral antagonism to identify critical host factors that govern disease outcome. Utilizing a systems-based approach, we examined differential regulation of IFN-γ–dependent genes following infection with robust respiratory viruses including influenza viruses [A/influenza/Vietnam/1203/2004 (H5N1-VN1203) and A/influenza/California/04/2009 (H1N1-CA04)] and coronaviruses [severe acute respiratory syndrome coronavirus (SARS-CoV) and Middle East respiratory syndrome CoV (MERS-CoV)]. Categorizing by function, we observed down-regulation of gene expression associated with antigen presentation following both H5N1-VN1203 and MERS-CoV infection. Further examination revealed global down-regulation of antigen-presentation gene expression, which was confirmed by proteomics for both H5N1-VN1203 and MERS-CoV infection. Importantly, epigenetic analysis suggested that DNA methylation, rather than histone modification, plays a crucial role in MERS-CoV–mediated antagonism of antigen-presentation gene expression; in contrast, H5N1-VN1203 likely utilizes a combination of epigenetic mechanisms to target antigen presentation. Together, the results indicate a common mechanism utilized by H5N1-VN1203 and MERS-CoV to modulate antigen presentation and the host adaptive immune response.**

antigen presentation | epigenetics | coronavirus | influenza | DNA methylation

Since the beginning of the new century, the emergence of novel influenza and coronavirus (CoV) strains has led to significant pandemics and poses a continuing threat to global public health (1–3). Understanding how these respiratory pathogens induce disease is key for treatment and prevention strategies (1). For successful respiratory viruses, multiple elements of the host immune response must be overcome, including both innate and adaptive immunity (1, 3). While these immune mechanisms are relatively conserved, complex interactions govern disease outcome, and successful viruses use a combination of approaches to combat host immunity. Even among related viruses, diverse strategies may produce similar infection results through distinct mechanisms (4). Therefore, susceptibility to a host pathway may not be uniform across a viral family or apply to all viruses infecting the same tissue. In exploring these responses, cross-comparisons may identify common strategies used by different viruses to antagonize the host immune responses. In our approach, we sought to leverage differences and similarities between respiratory pathogens to identify novel viral antagonism strategies (5).

Previously, our group used a combination of virologic, transcriptomic, and proteomic data to identify differences in the global type I IFN-stimulated gene (ISG) response across infections with A/influenza/California/04/2009 (H1N1; herein H1N1-09), A/influenza/

## Significance

Both highly pathogenic avian influenza virus and Middle East respiratory syndrome coronavirus (MERS-CoV) infections are characterized by severe disease and high mortality. The continued threat of their emergence from zoonotic populations underscores an important need to understand the dynamics of their infection. By comparing the host responses across other related respiratory virus infections, these studies have identified a common avenue used by MERS-CoV and A/influenza/Vietnam/1203/2004 (H5N1-VN1203) influenza to antagonize antigen presentation through epigenetic modulation. Overall, the use of cross-comparisons provides an additional approach to leverage systems biology data to identify key pathways and strategies used by viruses to subvert host immune responses and may be critical in developing both vaccines and therapeutic treatment.

Author contributions: V.D.M., A.S., A.J.E., Y.K., and R.S.B. designed research; V.D.M., A.S., A.J.E., K.B.W., L.E.G., and A.C.S. performed research; V.D.M., A.S., K.E.B.-J., H.D.M., C.D.N., S.O.P., C.P.C., M.E.M., K.K.W., K.G.S., B.-J.M.W.-R., T.O.M., R.D.S., and K.M.W. analyzed data; and V.D.M., A.S., and R.S.B. wrote the paper.

Reviewers: C.B., Cleveland Clinic; B.G.H., Arizona State University; and V.J.M., NIH.

Conflict of interest statement: Y.K. has received speaker's honoraria from Toyama Chemical and Astellas Inc.; and grant support from Chugai Pharmaceuticals, Daiichi Sankyo Pharmaceutical, Toyama Chemical, Tauns Laboratories, Inc., and Otsuka Pharmaceutical Co., Ltd. Y.K. is a founder of FluGen.



Data deposition: Raw microarray data reported in this paper have been deposited in the Gene Expression Omnibus (GEO) database, https://www.ncbi.nlm.nih.gov/geo (accession nos. GSE33267, GSE37571, GSE28166, and GSE45042). CHIP-Seq, MeDIP-Seq, and raw proteomics data have been made available on the Omics-LHV web portal, https://omics-lhv.org/data/ (experiment nos. ICL104, ICL105, MCL004, and MCL005). Raw proteomics data corresponding to peptide identifications used to populate the AMT tag database are available at the PRoteomics IDEntification (PRIDE) database, https://www.ebi.ac.uk/pride/ (accession nos. 19877–19890). The raw quantitative proteomics data can be accessed at the Pacific Northwest National Laboratory Biological Mass Spectrometry Data and Software Distribution Center (omics.pnl.gov/) in the Systems Virology Contract Data folder within the Browse Available Data folder.

[1]V.D.M. and A.S. contributed equally to this work.

[2]Present address: Drug Development Division, Southern Research, Frederick, MD 21701.

[3]A.C.S., Y.K., and R.S.B. contributed equally to this work.

[4]To whom correspondence may be addressed. Email: yoshihiro.kawaoka@wisc.edu or rbaric@email.unc.edu.

This article contains supporting information online at www.pnas.org/lookup/suppl/doi:10.1073/pnas.1706928115/-/DCSupplemental.

Vietnam/1203/2004 (H5N1; herein H5N1-VN1203), severe acute respiratory syndrome CoV (SARS-CoV), and Middle East respiratory syndrome CoV (MERS-CoV) (6). Our results found that a subset of ISGs was down-regulated by both H5N1-VN1203 and MERS-CoV, despite intact host signaling and transcriptional factor activation. Importantly, repressive histone markers were associated with down-regulated genes and suggested that both MERS-CoV and H5N1-VN1203 use epigenetic modifications to modulate ISG stimulation. These results correspond with reports for other viruses and suggest epigenetics as a new horizon for viral antagonism (7, 8).

In this study, we expanded upon our previous approach to explore IFN-γ–dependent gene expression following pathogenic influenza and CoV infection (6). Dividing differentially expressed genes by function, we observed down-regulation of IFN-γ–associated antigen-presentation gene expression following both H5N1-VN1203 and MERS-CoV infection. When all major histocompatibility complex (MHC) molecules and antigen-presentation genes were considered, the data demonstrated global down-regulation of gene expression that was confirmed by proteomic analysis. However, in contrast to the mechanisms controlling ISG expression (6), analysis of histone modifications did not reveal Increases in either activating or repressive markers following MERS-CoV infection. Instead, changes in DNA methylation likely facilitate MERS-CoV–mediated down-regulation of antigen-presentation molecules. For H5N1-VN1203, both histone modification and DNA methylation may play a role through the activity of viral NS1. In contrast, MERS-CoV accessory ORF mutants maintain gene expression down-regulation despite robust attenuation in virus growth. Together, these results highlight epigenetic modification as an important means by which respiratory viruses modulate host immunity.

## Results

Having previously identified type I IFN-dependent genes specific to the human airway epithelial cell line Calu3 cells (6), the same approach was applied to define genes responsive to IFN-γ. While some reports have indicated production by epithelial cells (9), RNA expression data indicated no IFN-γ signal following infection of Calu3 cells. However, responses to IFN-γ have been shown to be critical in the innate and adaptive immune response to respiratory infection, and epithelial cell IFN-γ responses may play a key role during infection (10–14). Calu3 cells, treated with recombinant IFN-γ, induced differential expression (DE) of 426 genes [logtwofold change (FC) of >1.5, adjusted $P$ value < 0.05]. Using these data, we developed a consensus IFN-γ–responsive list from the 136 genes induced at more than one time point (Table S1). While significant overlap was observed with type I IFN-responsive genes (42 of 136, 31%) (6), consensus IFN-γ genes also induced transcription factors, apoptosis/cell survival genes, ubiquitination machinery, and genes within other functional categories (Table 1). The consensus IFN-γ gene list was then used to examine expression changes following infection with successful respiratory viruses. Despite the absence of IFN-γ signal in these cultures, infection with influenza H1N1-09, H5N1-VN1203, SARS-CoV, and MERS-CoV induced expression of IFN-γ–responsive genes by other factors; however, these IFN-γ–responsive gene expressions varied across viral infections, despite similar kinetics of replication (Fig. 1). For H1N1-09 and SARS-CoV, the majority of IFN-γ–responsive genes were strongly up-regulated, with only ∼10% exhibiting down-regulation. In contrast, >40% of these same genes were down-regulated by H5N1-VN1203 and MERS-CoV. Examining the IFN-γ–responsive genes by functional subsets revealed multiple gene groups targeted for down-regulation (Table 1). Most notable for both H5N1-VN1203 and MERS-CoV infection were genes associated with antigen presentation, including several MHC molecules; 80% or more of the IFN-γ–responsive genes associated with antigen presentation were down-regulated following H5N1-VN1203 or MERS-CoV infection (Table 1). In contrast, <10% of these genes were down-regulated following either H1N1-09 or SARS-CoV infection. Together, the results suggest strong down-regulation of antigen-presentation genes following both H5N1-VN1203 and MERS-CoV infection.

**Table 1. Down-regulated IFN-γ–responsive genes by classification**

| | Percentage of down-regulated type II IFN consensus genes by category | | | |
|---|---|---|---|---|
| Category | H5N1, % | H1N1, % | SARS, % | MERS, % |
| Apoptosis | 60 | 40 | 0 | 60 |
| Complement | 57.1 | 0 | 14.3 | 54.1 |
| Cytokine | 11.1 | 11.1 | 11.1 | 33.3 |
| Lipid proteins | 67 | 22.2 | 33.3 | 88.9 |
| **MHC** | **86.7** | **6.6** | **6.6** | **80** |
| ISG | 18.2 | 0 | 0 | 18.2 |
| Nucleotide binding proteins | 37.5 | 0 | 0 | 37.5 |
| Receptors | 66.7 | 33.3 | 0 | 50 |
| Transcriptional factors | 60 | 10 | 0 | 30 |
| Ubiquitin | 60 | 0 | 0 | 40 |
| Unclassified | 35.2 | 29.4 | 23.5 | 58.8 |

IFN-γ–responsive gene divided into functional categories and classified as either up-regulated (log2 FC > 0) or down-regulated (log2 FC < 0). Boldface, MHC and antigen presentation-related molecules had >80% down-regulation in both H5N1-VN1203 and MERS-CoV ($n$ = 15 genes).

**Down-Regulation of Antigen-Presentation Gene Expression and the MHC Locus.** We next sought to determine whether down-regulation of antigen presentation was limited to IFN-γ–responsive genes or could be detected across the entire spectrum of antigen-presentation molecules. Therefore, we next examined gene expression of both MHC molecules and other components associated with antigen presentation; the majority of these genes were located within the MHC locus on human chromosome 6 (chr. 6), while others were interspersed throughout the genome (Table S2). The results indicated broad down-regulation of antigen-presentation molecules following both H5N1-VN1203 and MERS-CoV infection (Fig. 2). In contrast, H1N1-09 infection had no effect or strongly increased expression of these genes; similarly, SARS-CoV also induced expression for the majority of these genes. Globally, both H5N1-VN1203 and MERS-CoV infection resulted in reduced expression of both MHC class I and II molecules. Similarly, the expression of other genes involved in antigen presentation, including transcription factors (*CTIIA*) and machinery (*TAP2* and *PDIA3*), both in the MHC locus and on other chromosomes (distant), was also strongly down-regulated. Importantly, while adjacent genes on chr. 6 not involved in antigen presentation and MHC class III genes (complement, TNF, etc.) had some modulation, down-regulation was not uniform, suggesting specific targeting of MHC and antigen-presentation molecules by both H5N1-VN1203 and MERS-CoV.

**Proteomics Confirms Broad Down-Regulation of Antigen-Presentation Genes.** In parallel to RNA expression analyses, antigen-presentation components were examined within the context of global proteomics. As expected, peptides associated with antigen-presentation-related molecules were detected in baseline mock-infected proteomic samples. Consistent with transcriptomic data, peptides mapping to class I MHC proteins (HLA-A, -B, or -C) exhibited statistically significant decreases after MERS-CoV or H5N1-VN1203 infection, but were significantly increased in cells infected with SARS-CoV or H1N1-09 (Fig. 3). Interestingly, while MERS-CoV infection strongly down-regulated HLA-A, -B, and -C peptides, H5N1-VN1203 infection consistently down-regulated HLA-A and -C, but not HLA-B, peptides (Fig. 3). Peptides

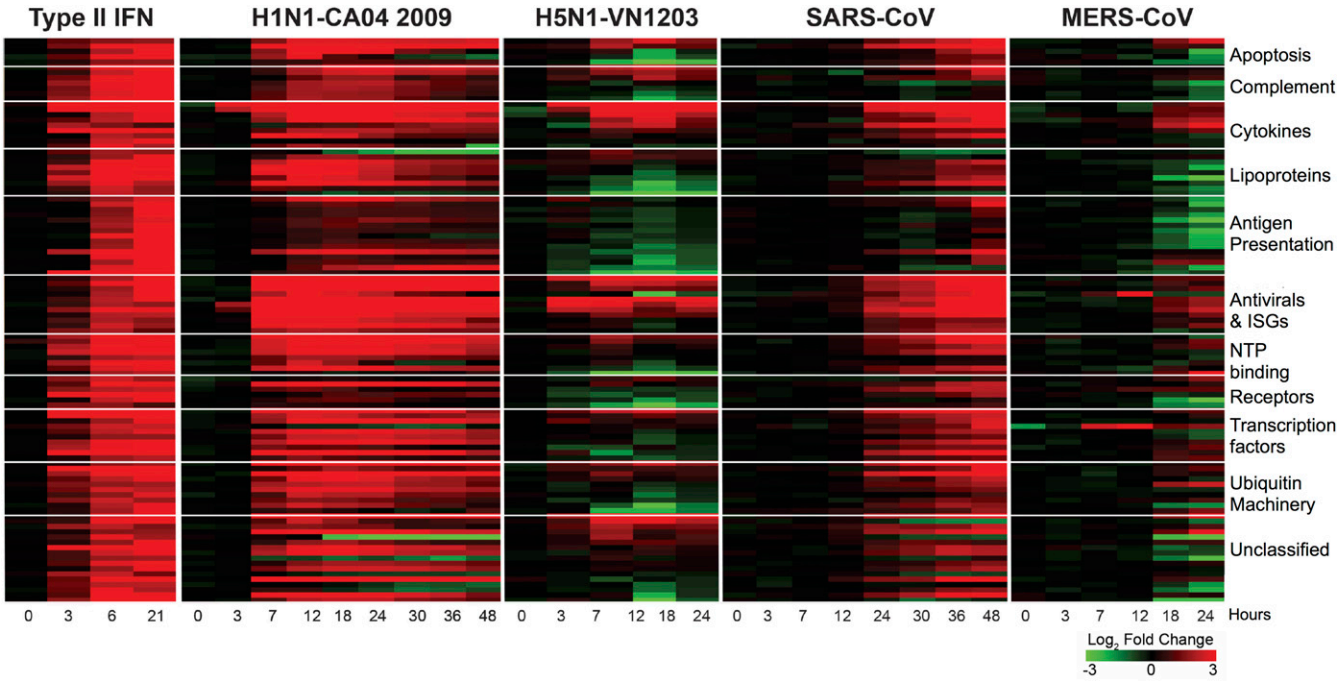


**Fig. 1.** Type II IFN treatment and diverse respiratory virus infections result in robust expression differences. Global transcriptional response of consensus genes following IFN-γ treatment or infection with H5N1-VN1203, H1N1-09, SARS-CoV, and MERS-CoV is shown. Genes were ordered by functional groups. Values represent logtwofold change compared with time-matched mock-infected samples.

associated with other (non-HLA) antigen-presentation proteins exhibited similar overall expression patterns (Fig. 3*A*). Together, the transcriptomic and proteomic data indicate that antigen-presentation molecule expression is antagonized by MERS-CoV and H5N1-VN1203 infections—with some potential differences in efficiency or mechanism of antagonism—but not by SARS-CoV and H1N1-09 infections.

**Histone Modification Does Not Drive MERS-CoV–Mediated MHC Down-Regulation.** Previously, we demonstrated that a subset of type I ISGs are down-regulated by H5N1-VN1203 and MERS-CoV infections, and our results implicated alterations in histone modification in driving differential ISG expression (6). To determine whether histone modifications also affect antigen-presentation gene expression, we examined enrichment of activating (H3K4me3) and repressive (H3K27me3) methylation markers on the 5′ promoters of MHC class I (HLA-A), II (HLA-DRB), and III (LTA) molecules in lysates from cells infected with SARS-CoV, MERS-CoV, H5N1-VN1203, or H1N1-09 using a chromatin immunoprecipitation-PCR (ChIP-PCR)–based approach. For the activating histone marker (H3K4me3), enrichment was observed only in HLA-A promoter regions following H1N1-09 and H5N1-VN1203 infection, and no enrichment or loss of H3K4 trimethylation was observed for HLA-DRB1 or LTA promoters following either influenza virus infection (Fig. 4*A*). SARS-CoV infections did not result in significant enrichment or loss of H3K4me3 for any of these genes. In contrast, MERS-CoV infection reduced H3K4 trimethylation for all three genes, with significant changes observed in HLA-DRB1 and LTA promoter regions. For all three promoter regions, strong reductions in the repressive marker (H3K27me3) were also observed following SARS-CoV and MERS-CoV infections (Fig. 4*B*); similarly, H1N1-09 and H5N1-VN1203 also reduced repressive marks for the HLA molecules. Together, the data suggest that modest transcriptional activation was possible if H3K4me3 motifs remained intact.

To expand on this these findings for high-pathogenicity viruses (H5N1-VN1203 and MERS-CoV), we next performed ChIP-sequencing (ChIP-seq) analysis for H3K4me3 and H3K27me3 and identified histone modification patterns for all genes on chr. 6, which contains the MHC locus. In H5N1-VN1203 infections, we observed depletion of H3K4 trimethylation across the length of chr. 6, with the strongest depletion in parts of the MHC locus (Fig. 4*C*). Concurrently, few chr. 6 genes exhibited substantial depletion of H3K27 trimethylation (Fig. S1*A*), and some were enriched for H3K27me3 (Fig. S1*B*). Taken together, these

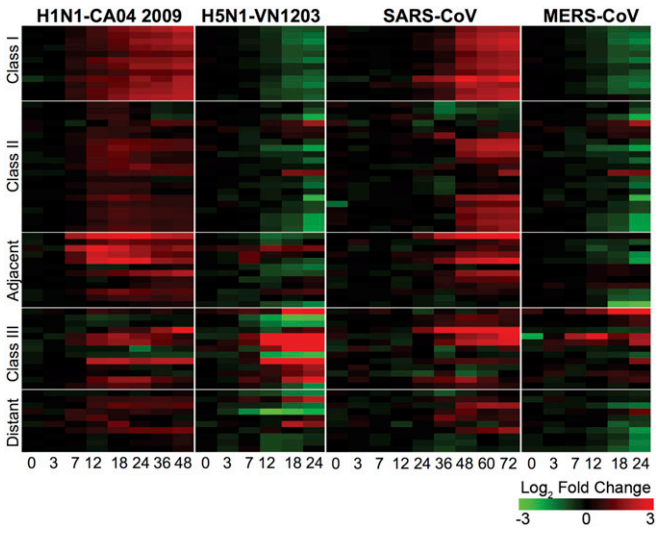


**Fig. 2.** Both H5N1-VN1203 and MERS-CoV down-regulate genes within the MHC locus and associated with antigen presentation. Global transcriptional response of gene located within the MHC locus on chr. 6 (MHC class I, II, III, and adjacent genes) or distant genes (not located on chr. 6) associated with antigen presentation following infection with H5N1-VN1203, H1N1-09, SARS-CoV, and MERS-CoV is shown. Genes are ordered by MERS-CoV expression levels at 24 hpi. Values represent logtwofold change compared with time-matched mock-infected samples.

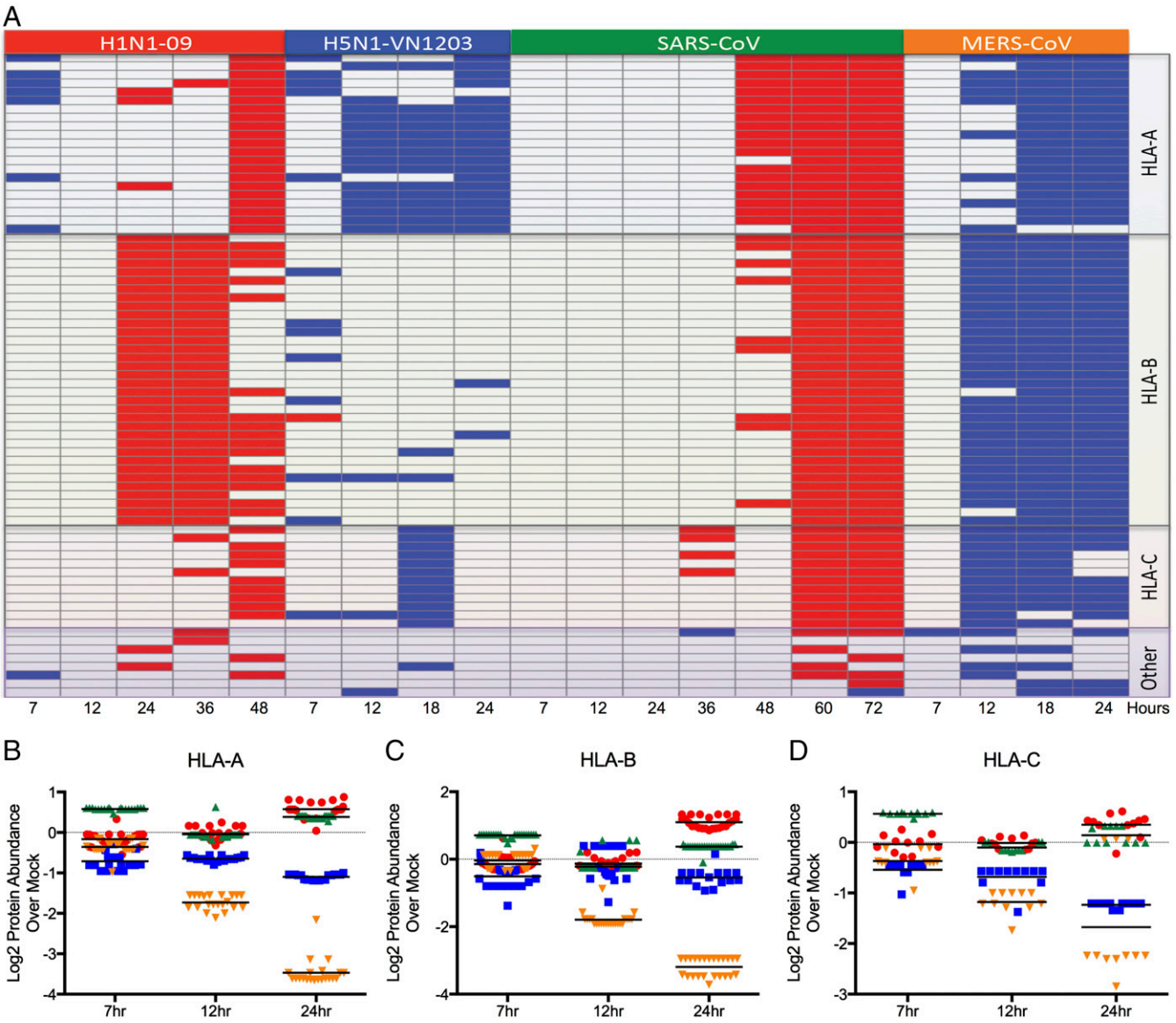


**Fig. 3.** Proteomics analysis confirmed down-regulation of MHC class I-associated molecules following H5N1-VN1203 and MERS-CoV infection. (*A*) Differential abundance analysis comparing virus to time-matched mock samples with statistically significant increases represented in red and decreases in blue (*P* values based on logtwofold changes, flagged for statistical significance based on $P \leq 0.05$). *P* values are derived from ANOVA (quantitative comparison) when enough data are present; otherwise, *P* values are from the g test (qualitative comparison). (*B–D*) Peptide abundance normalized to mock for HLA-A (*B*), HLA-B (*C*), and HLA-C (*D*) molecules following infection with H1N1-09 (red), H5N1-VN1203 (blue), SARS-CoV (green), and MERS-CoV (orange). Each point represents peptide associated with an HLA molecule class and line plotted for average of multiple peptides.

observations suggest that H5N1-VN1203 infection may reduce the potential for transcriptional activation of chr. 6 genes, particularly within the MHC locus, and further implies that histone alterations may contribute to H5N1-VN1203–mediated down-regulation of antigen-presentation gene expression. For MERS-CoV, histone modification data offer a muddled picture, with enrichment and depletion found for both activating and repressive markers (Fig. S1). Coupled with the ChIP-PCR of the promoter regions, these results suggest that histone modifications are not the driver of MERS-CoV–mediated antagonism of antigen presentation.

**DNA Methylation Contributes to Antagonism of Antigen Presentation.** While reduced histone modifications following MERS-CoV infection failed to explain down-regulation of antigen-presentation molecules, it suggested an alternative epigenetic mechanism: DNA methylation. Direct methylation of genomic DNA functionally ablates expression, indirectly leading to reduced access and loss of histone marks. To examine this possibility, we performed methylated DNA-IPs (MeDIPs) with virus-infected cells and then assessed the methylation status of three antigen-presentation-associated gene promoters (*HLA-A*, *B2M*, and *PDIA3*) using PCR (Fig. 5*A*). For H1N1-09, infection resulted in modest changes, with increased methylation of HLA-A and reduced methylation of B2M promoter regions. Similarly, SARS-CoV infection generally resulted in modest DNA methylation trending toward reduced methylation relative to mock-infected controls. In contrast, H5N1-VN1203 infection increased methylated DNA levels in the same target genes, and, strikingly, MERS-CoV infection resulted in complete methylation (100%) of all three target genes. To verify the effect observed in MERS-CoV infections, we performed MeDIP-PCR reactions for three additional antigen-presentation gene promoters (*CIITA*, *HLA-E*, and *PSMB9*) and again observed complete promoter

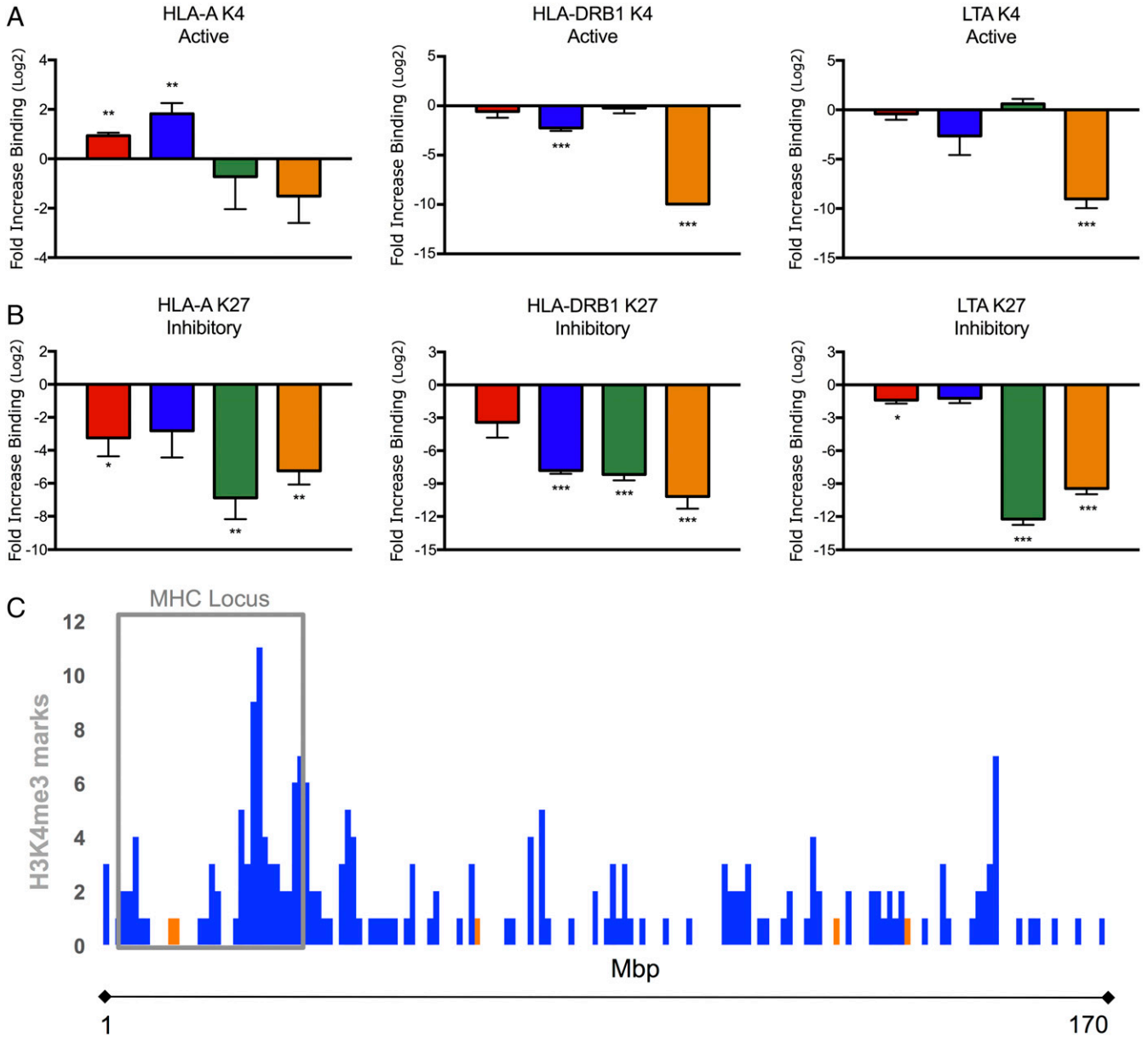


**Fig. 4.** Altered histone modifications play a role in H5N1-VN1203 influenza, but not MERS-CoV antagonism of antigen presentation. (*A* and *B*) ChIP with antibodies against H3K4me3 (*A*) or H3K27me3 (*B*) followed by qPCR of the 5′ UTR of the identified genes 18 hpi with H1N1-09 (red), H5N1-VN1203 (blue), SARS-CoV (green), or MERS-CoV (orange). Values represent fold increase binding compared with mock on Log2 scale. *P* values are based on Student's *t* test and compare individual viral infection to mock value: $*P < 0.05$; $**P < 0.01$; $***P < 0.001$. (*C*) Chromosome plot of chr. 6 showing depletion of H3K4 methylation following H5N1-VN1203, but not MERS-CoV, infection. Loss of H3K4 methylation was called against the time-matched mock reads as reference reads with mock values equaling 0. H3K4 methylation depletion was then quantified and plotted as bars according the location on chr. 6; each bar indicates total number of histone modification marks within 1 Mb.

methylation for all genes (Fig. S2). Global methylation analysis of chr. 6 revealed robust methylation across the entire chromosome following MERS-CoV infection (Fig. 5*B*). Importantly, while H5N1-VN1203 infection also induced increased methylation across chr. 6, its peaks were less in magnitude than observed in MERS-CoV infection.

However, it is possible that DNA methylation is due to stress induced by viral infection. Both MERS-CoV and H5N1-VN1203 produced significant cytopathic effect by 24 h postinfection (hpi), contrasting both SARS-CoV and H1N1-09. However, while a global increase in methylation was observed following MERS-CoV and H5N1-VN1203 infection, it was far from uniform across the entire genome. More in-depth analysis of methylation data found that, following MERS-CoV infection, the ∼3.464-Mbp MHC locus maintained 49.11 meCpGs/Mbp. In contrast, the remainder of chr. 6 averaged 19.54 meCpGs/Mbp following MERS-CoV infection. Similarly, examination of other chromosomes (Table S3) found lower meCpG/Mbp rates, suggesting specificity in the magnitude of DNA methylation at the MHC locus and potentially other genomic locations. Similarly, H5N1-VN1203 methylation within the MHC locus corresponded to 34.29 meCpG/Mbp vs. 7.7 meCpG/Mbp over the remainder of the chr. 6. Together, these results suggest that DNA methylation is at least one of the primary mechanisms exploited by MERS-CoV to antagonize antigen-presentation gene expression in infected cells, while H5N1-VN1203 may use a combination of DNA methylation and histone-modification alterations to achieve a similar affect.

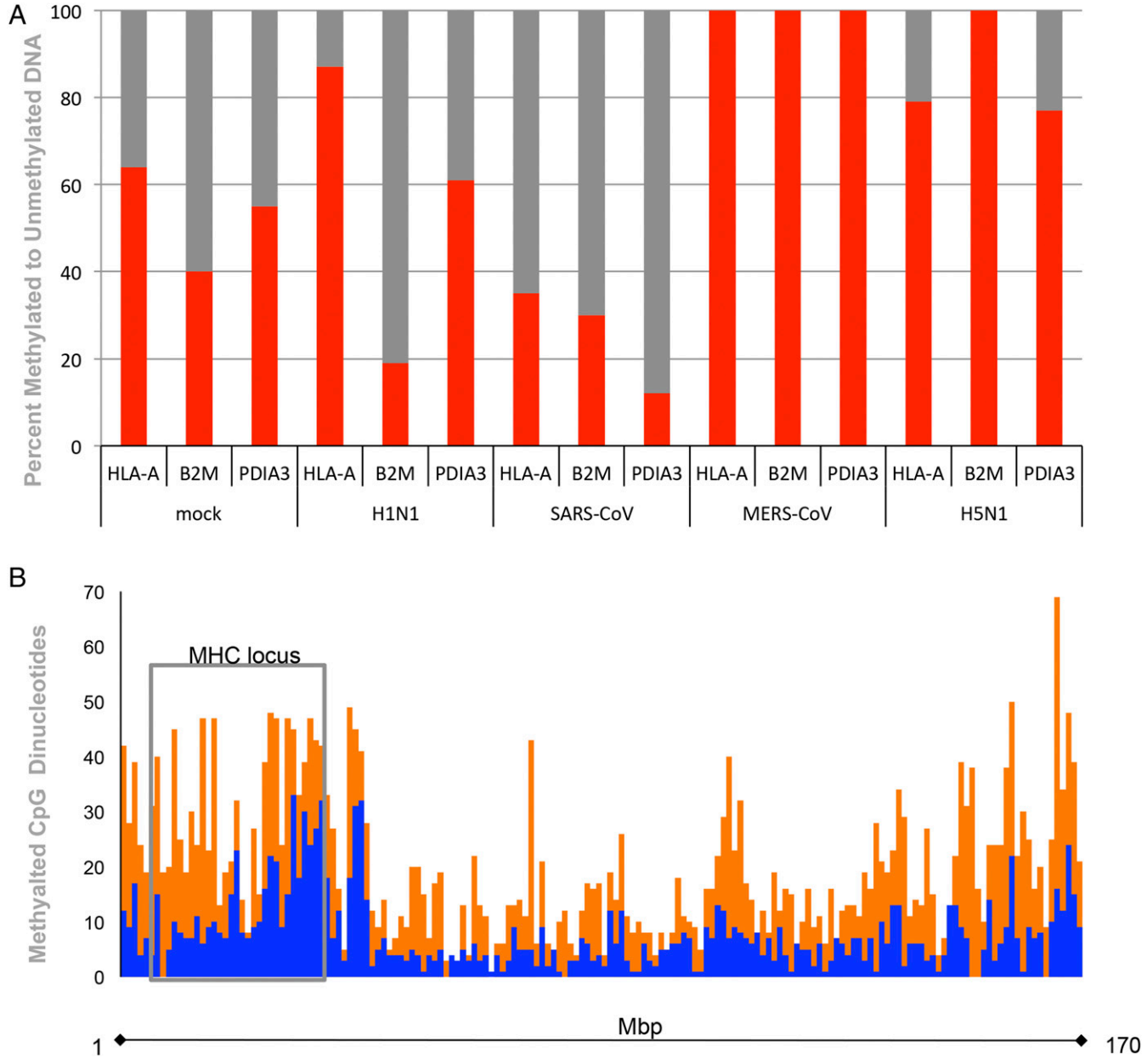





**Fig. 5.** Examination of host DNA revealed complete methylation at MHC gene loci following MERS-CoV infection. (*A*) DNA methylation status during MERS-CoV, SARS-CoV, H5N1, and H1N1 infection. MeDIP was performed with total DNA from Calu3 cells infected with MERS-CoV, SARS-CoV, H5N1-VN1203, or H1N1-09 for 18 h to determine the methylation status of MHC gene promoters. Methylated CpG islands within the promoter regions for *HLA-A*, *B2M*, and *PDIA3* were quantified by qRT-PCR. Results were reported as relative percentage of methylated (red) and unmethylated (gray) DNA in each target genomic DNA sequence for each virus. (*B*) Chromosome plot of chr. 6 showing DNA methylation after H5N1 and MERS-CoV infection. Differential methylation levels were called against the time-matched mock reads as reference reads with mock values equaling 0. Methylation levels were then quantified and plotted as bars according their location on chr. 6; each bar indicates the total number of differential methylation marks within 1 Mb.

**Both Viral and Host Processes Contribute to DNA Methylation.** To examine how these respiratory viruses target antigen presentation via epigenetic modulation, we utilized MERS-CoV and H5N1-VN1203 mutants that lacked key viral proteins. Previous work by our group implicated influenza NS1 in histone modification and ISG down-regulation compared with a similarly replication attenuated PB2 mutant (6). In this study, we extended this analysis to antagonism of antigen-presentation molecules. Following infection of Calu3 cells with wild-type (WT), C-terminal truncation of NS1 (NS1trunc124), or PB2 encoding an amino acid substitution (PB2-K627E) mutant viruses, we examined changes in viral replication as well as HLA-A and -C peptide abundance (Fig. 6 *A* and *B*). While the overall peptide level was decreased relative to mock, truncation of H5N1-VN1203 NS1 resulted in augmented protein expression of both MHC class I molecules relative to the WT virus. Importantly, the reduction of MHC class I down-regulation was not a product of attenuated viral replication, as the PB2 mutant had similar replication kinetics and titer, but maintained HLA-A and -C antagonism (Fig. S3*A*). Together, the results implicate a role for NS1 in modulation of antigen presentation following H5N1-VN1203 infection.

In contrast, results from an attenuated MERS accessory ORF mutant virus infection suggested that host processes may contribute to the modulation of host antigen presentation. The

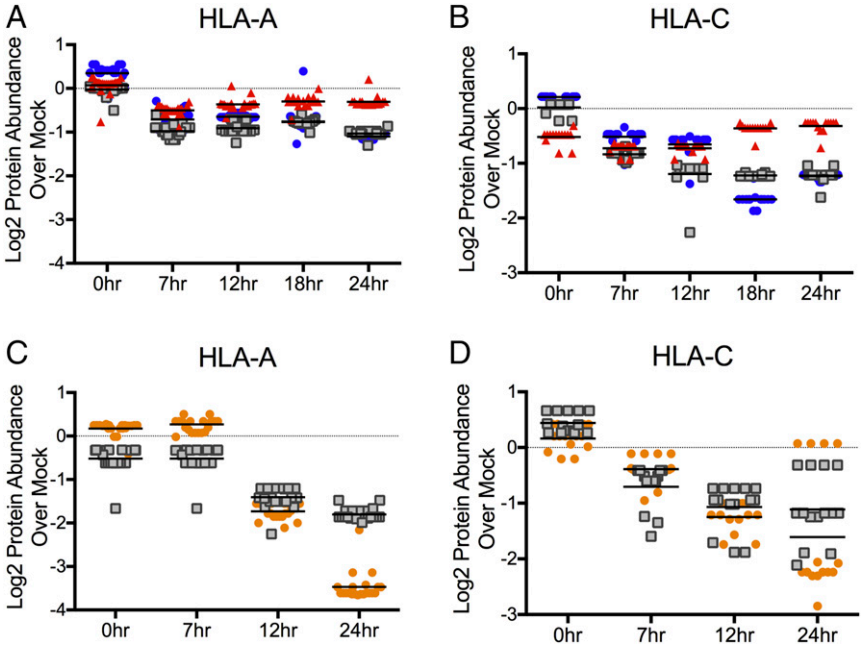


**Fig. 6.** Proteomics analysis of H5N1-VN1203 and MERS-CoV mutants suggest that both viral and host processes contribute to reduction of antigen-presentation molecules. (*A* and *B*) Peptide abundance normalized to mock for HLA-A (*A*) and HLA-C (*B*) following infection with influenza H5N1-VN12033 WT (blue), PB2-K627E mutant (gray), or NS1-truncation (red). (*C* and *D*) Peptide abundance normalized to mock for HLA-A (*C*) and HLA-C (*D*) following infection with MERS-CoV WT (orange) or accessory ORF mutant (ΔORF3-5; gray). Each point represents a peptide associated with an HLA molecule class and line plotted for average of multiple peptides.

absence of MHC locus antagonism in SARS-CoV and other CoV infection suggested that a nonconserved portion of the MERS-CoV backbone is involved. With this in mind, we focused on the MERS-CoV accessory ORF proteins, which have limited sequence similarities with other CoV family proteins. Using a previously described MERS-CoV mutant that deletes all four accessory ORFs (d3-5) (15), we infected Calu3 cells and examined both viral replication and proteomics. Following infection, the d3-5 mutant virus produced robust attenuation in terms of viral replication (Fig. S3*B*). However, despite a nearly 100-fold reduction in viral replication, the d3-5 mutant viruses maintained strong down-regulation of MHC class I molecules HLA-A and -C (Fig. 6 *C* and *D*). While not equivalent to WT MERS-CoV down-regulation, the d3-5 mutant maintained lower absolute MHC class I peptide abundance compared with WT H5N1-VN1203 (Fig. 6 *A* and *B*). Together, the data suggest that even a robustly attenuated MERS-CoV mutant can stimulate down-regulation of antigen-presentation molecules and potentially implicate host processes in contributing to reduction of MHC class I molecules following infection.

## Discussion

System-based analysis has previously revealed similarities and contrasts in terms of ISG induction between and within viral families (6). This study extends that approach, demonstrating DE of IFN-γ–dependent genes following H1N1-09, H5N1-VN1203, SARS-CoV, and MERS-CoV infection. Expanding on the initial comparison, analysis of functional categories demonstrated global down-regulation of MHC and antigen-presentation molecules following both MERS-CoV and H5N1-VN1203 infection; these results correspond to MHC down-regulation reported for H5N1 in A549 and chicken embryonic fibroblasts (16, 17). The changes in RNA expression were found throughout the MHC locus and were confirmed by proteomic analysis in both viruses. Seeking mechanistic insights, epigenetic studies captured robust increases in DNA methylation following MERS-CoV infection with no similar trend observed following mock or SARS-CoV infection. However, while H5N1-VN1203 had augmented DNA methylation relative to mock, its overall increase was less uniform than MERS-CoV, leaving the possibility that histone modification may also contribute to control of antigen-presentation gene expression. Together, the data from both MERS-CoV and H5N1-VN1203 infection suggest that multiple epigenetic mechanisms contribute to antagonism of the host immune response.

While not definitive, mutant virus data suggest that both viral proteins and host processes may modulate antigen presentation following MERS-CoV and H5N1-VN1203 infection. Similar to down-regulation of ISGs (6), truncation of H5N1-VN1203 NS1 resulted in augmentation of MHC class I molecules relative to WT infection; importantly, the reduction was not a simple product of lower viral replication, as a similarly attenuated viral mutant maintained down-regulation of MHC class I molecules. In contrast, a MERS-CoV mutant strain lacking all four accessory ORF proteins produced robust down-regulation of both HLA-A and -C, despite a 100-fold replication attenuation relative to WT control virus. These results suggest that MERS-CoV entry or initial steps of infection trigger antagonism of antigen presentation. One possibility is stimulation of host processes that directly or indirectly result in reduction of the antigen-presentation molecules. For example, MERS-CoV infection may stimulate depression of host gene regulation, resulting in increased competition for transcription factors driving MHC expression. Alternatively, activation of DNA methylation pathways may be initiated by MERS-CoV infection, resulting in regulation of host constitutive processes as well as dipeptidyl peptidase 4 receptor expression (18). Together, the mutant virus data from both viruses suggest that complex host–pathogen interaction dictate epigenetic-based antagonism of antigen presentation.

Targeting of host antigen presentation has significant implications for pathogenesis of both MERS-CoV and H5N1-VN1203. Unlike SARS-CoV infection, which is limited to pneumocytes and ciliated airway epithelium in the lung (19), MERS-CoV has broader

tropism, infecting not only nonciliated airway epithelial cells and type 1/2 pneumocytes in the lung, but a number of immune cell populations, including T cells, macrophages, and dendritic cells in vitro (20–22); similarly, a number of H5N1-VN1203 strains have been reported to infect both macrophages and dendritic cells in vitro (23, 24). In the context of antigen presentation, the expanded tropism of both viruses potentially impacts systemic aspects of adaptive immunity and memory responses. For H5N1 strains, modulation of antigen presentation may contribute to the inefficacy of the CD8 T-cell response during acute infection (25) and marginal, waning memory responses overall (26). Similarly, MERS-CoV infection has been characterized by uneven and often marginal antibody serum neutralization in recovering patients (27, 28). For both viruses, manipulation of antigen presentation may contribute to these diminished responses and may have important ramifications for both vaccine designs.

For viral antagonism, the epigenetic landscape represents a potent and important avenue to disrupt the host immune response (29). While always a consideration for DNA viruses that reside in the nucleus, recent research has focused on how viruses utilize aspects of the epigenetic machinery to enable persistence and emergence (30). In addition, several reports have highlighted how viruses have disrupted epigenetic regulation and impact the host immune response. For example, NS1 of influenza H3N2 has been implicated as a histone mimic disrupting the antiviral response (8). Similarly, both hepatitis C virus and adenoviruses have proteins that interfere with epigenetics functions and alter global immune function (7, 31, 32). Previous work by our group found clear association of repressive histone modification H3K27me3 with down-regulated ISGs following both MERS-CoV and H5N1-VN1203 infection (6); subsequently, despite pathway and transcription factor activation, the repressed state physically prevented transcription of these genes. Similarly, our results in this work argue that DNA methylation plays a similar role in the loss of antigen-presentation molecules following both MERS-CoV and H5N1-VN1203 infection. Importantly, the sequencing data suggest that other specific regions of the genome are also targeted by global methylation, potentially signifying critical pathways modulated by viral antagonism and providing a path for future studies. In addition, viruses may utilize distinct epigenetic mechanism in parallel, resulting in specific targeting of host ISGs by H3K27 trimethylation instead of DNA methylation within that genome region. Together, these results suggest that multiple viruses target different epigenetic processes to modulate aspects of host immunity and indicate that additional studies will be required to fully understand how epigenetics modulates the host immune response following virus infection.

The data in this work highlight the utility of leveraging viral cross-comparisons as a way to identify host factors impacting disease outcomes. Convergent evolution predicts that diverse viruses will utilize similar and divergent strategies to overcome common host immune responses to produce successful infections (33). Therefore, in leveraging available systems-based datasets, we seek similarities and contrast between viruses while taking advantage of uniform platforms, infection conditions, and data collection methods (34). The results have provided insights into both MERS-CoV and H5N1-VN1203 manipulation of IFN responses and antigen presentation. These findings provide not only a better understanding of the host response to infection, but also have the potential to aid in the development of treatment and prevention strategies. Future studies should expand these approaches to explore other specific aspects of immunity, including inflammatory responses, apoptosis, and autophagy. Similarly, viral cross-comparisons can also be integrated across data types as well as in vitro and in vivo systems as an additional metric for more traditional modeling approaches (35–38). Importantly, much of this analysis can occur on publicly available datasets, increasing both the utility and impact of already existing systems data (34, 39). Overall, surveying contrasts in host responses between viruses represents a powerful means to understand treatment and pathogenesis.

## Experimental Procedures

**Cells and Viruses.** Calu3 cells were utilized as described (37, 38, 40). Viral titrations and propagation of SARS-CoV, MERS-CoV, and influenza virus were performed in VeroE6, Vero-81, and Madin–Darby canine kidney (MDCK) cells by using standard methods. WT icSARS-CoV was derived from the R.S.B. laboratory's infectious clone constructs (41). MERS-CoV (EMC 2012 strain) was provided by Bart L. Haagmans, Erasmus Medical Center, Rotterdam, The Netherlands via material transfer agreement. H5N1-VN1203 was derived from a plasmid-based reverse-genetic system, and H1N1-09 was from WT stock; both were subsequently amplified in MDCK cells (42).

**Infections.** Experiments using H5N1-VN1203, SARS-CoV, or MERS-CoV were performed in containment laboratories at the University of Wisconsin–Madison or University of North Carolina–Chapel Hill as described (40, 41). Influenza and CoV infections were carried out at a multiplicity of infection (MOI) of 1 (H5N1-VN1203), 3 (H1N1-09), and 5 (SARS-CoV and MERS-CoV) for both WT and mutant viruses as described (37, 38, 40).

**RNA Isolation, Microarray Processing, and Identification of DE.** RNA isolation and microarray processing from Calu3 cells was carried out as described (40). DE was determined by comparing virus-infected replicates to time-matched mock replicates. Criteria for DE in determining the consensus ISG list were an absolute $\log_2$ fold change of >1.5 and a false discovery rate (FDR)-adjusted $P$ value of <0.05 for a given time point.

**Proteomics Reagents, Sample Preparation, Database Construction, and Data Processing.** Proteomics preparation was carried out as described (37). Detailed experimental approaches have been included in *Supporting Information*. Quality control processing was performed to identify and remove contaminant proteins, redundant peptides, peptides with an insufficient amount of data across the set of samples (43), and LC-MS runs that showed significant deviation from the standard behavior of all LC-MS analyses (44). Peptides were normalized by using a statistical procedure for the analysis of proteomic normalization strategies that identified the peptide-selection method and data-scaling factor which introduced the least amount of bias into the dataset (45). The peptide abundance values were normalized across the technical replicates by using a global median centering of the data. Normalized log10 abundance values were averaged across the technical replicates within each biological sample. Peptides were evaluated with a Dunnett adjusted $t$ test and a G test to identify quantitative and qualitative significance patterns, respectively, in the peptide data. Peptide level significance patterns were used for protein roll-up to select appropriate peptides for protein quantification. Proteins were quantified by using a standard R-Rollup method using the most abundant reference peptide (46) after filtering the peptides that were redundant, had low data content, or were outside the dominant significance pattern.

**ChIP-PCR.** ChIP analysis was performed by using the EpiTect ChIP OneDay Kit (Qiagen). Briefly, infected Calu3 cells were cross-linked, harvested, and frozen at −80 °C. Cells were then lysed and chromatin sheared via sonication to generate chromatin fragments between 250 and 1,000 base pairs. Sonicated samples were then immunoprecipitated with anti-STAT1 (clone C-24; Santa Cruz Biotechnology), anti-H3K4me3 (Qiagen), anti-H3K27me3 (Qiagen), or anti-mouse IgG (Qiagen) as a control. To determine the histone modification distribution, quantitative real-time PCR (qPCR) was performed by targeting the 5′ UTR (−750 bp to transcription start site) of select genes; target and primer information are included in *Supporting Information*. ChIP results were reported as fold difference (or differential occupancy), allowing comparison across multiple samples. For this, each sample was normalized to the input, and then the fold enrichment was calculated by using the ΔΔCt method. The fold difference for each gene was determined by dividing the appropriate time-matched mock by the experimental group. Finally, the fold difference values were converted to log2 and plotted. Data presented are the means ± SEs for triplicate samples.

**ChIP-Seq.** ChIP analysis for NGS sequencing was performed by using the MAGnify ChIP System (Invitrogen). Briefly, for ChIP analysis, Calu3 cells were plated (~$1.5 \times 10^6$ per well) and infected with H5N1-VN1203 or H1N1-09 at an MOI of 5 and harvested at 0 and 12 hpi; cultures inoculated with PBS alone served as time-matched mock controls. Sonication conditions were

chosen to result in the desired size distribution of the sonicated chromatin between 250 and 1,000 bp. Sonicated samples were then immunoprecipitated with anti-H3K4me3 (Qiagen) and anti-H3K27me3 (Qiagen). To determine genome-wide histone modification, ChIP DNA was subjected to next-generation sequencing (NGS) on a TruSeq ChIP Library Preparation Kit (Illumina) and sequenced on an Illumina HiSeq. NGS data analysis was performed by utilizing the CLC Genomics Workbench. The Histone ChIP-Seq plugin provided analysis tools for a complete histone modification analysis. Briefly, paired end reads were mapped against the human GRCh37/hg19 reference genome by using a stringent alignment setting (mismatch cost = 2). Peaks were called against the time-matched mock reference reads. To determine specific genomic regions of histone modification enrichment, the maximum $P$ value for peak calling was set to $P < 0.05$ to detect regions that had a significant fit with the peak shape.

**MeDIP-PCR.** Briefly, for methylated DNA analysis, Calu3 cells were plated ($\sim 1.5 \times 10^6$ per well) and infected with MERS-CoV, SARS-CoV, H5N1-VN1203, or H1N1-09 at a MOI of 5 or 3 (H5N1 only). Total genomic DNA was harvested 0, 12, 18, and 24 hpi by using the PureLink Genomic DNA Minikit. Cultures inoculated with PBS alone served as time-matched mock controls. Sonication conditions were chosen to result in the desired size distribution of the sonicated total DNA between 250 and 1,000 bp. Sonicated samples were then used to enrich methylated DNA by using the methyl-CpG binding domain of human MBD2 protein (MethylMiner Methylated DNA Enrichment Kit; Invitrogen). To determine the methylation status of MHC gene promoters, qRT-PCR was performed. For this, primer pairs targeted the CpG islands of target genes. Results were reported as the relative percentage of methylated and unmethylated DNA in each target genomic DNA sequence by using the ΔΔCt method. The fraction methylated of DNA in each sample was calculated by normalizing the total DNA amount to the amount of unmethylated DNA.

**MeDIP-Seq.** To determine genome-wide methylation status, enriched methylated DNA was subjected to NGS. Genomic DNA was harvested as described above by pooling three samples, and libraries were generated by using the TruSeq DNA Methylation Kit (Illumina) and sequenced on an Illumina HiSeq. NGS data analysis was performed by utilizing the CLC Genomics Workbench. The Bisulfite Sequencing plugin provided analysis tools for a complete bisulfite sequencing workflow. Briefly, bisulfite paired-end reads were mapped against the human GRCh37/hg19 reference genome by using a stringent alignment setting (mismatch cost = 2). Methylation levels were called against the time-matched mock reads, and resulting methylation levels of sample and reference were compared by using a Fisher exact test ($P < 0.05$.) detecting differential methylation levels.

**Data Dissemination.** Raw microarray data for these studies were deposited in publicly available databases in the National Center for Biotechnology Information Gene Expression Omnibus (GEO) database (37) and are accessible through GEO accession no. GSE33267 (https://www.ncbi.nlm.nih.gov/geo/query/acc.cgi?acc=GSE33267). CHIP-Seq, MeDIP-Seq, and raw proteomics data have been made available on the Omics-LHV web portal (https://omics-lhv.org/data/). Raw proteomics data corresponding to peptide identifications used to populate the AMT tag database are available at the PRoteomics IDEntification (PRIDE) database (https://www.ebi.ac.uk/pride/archive/) under the project "A Systems Biology Approach to Emerging Respiratory Viral Diseases" in the PRIDE Public Projects folder and corresponding to PRIDE accession nos. 19,877–19,890. The raw quantitative proteomics data can be accessed at the Pacific Northwest National Laboratory (PNNL) Biological Mass Spectrometry Data and Software Distribution Center (omics.pnl.gov/) in the Systems Virology Contract Data folder within the Browse Available Data folder. All data sets and associated metadata have been submitted to Virus Pathogen Resource (www.viprbrc.org/brc/home.spg?decorator=vipr).

**ACKNOWLEDGMENTS.** This research was supported by grants from NIH National Institute of Allergy and Infectious Diseases Grants U19AI100625 (to R.S.B.) and U19AI106772 (to Y.K.), and NIH National Institute of Aging Grant K99AG049092 (to V.D.M.). The content is solely the responsibility of the authors and does not necessarily represent the official views of the NIH. Proteomic analyses were performed in the Environmental Molecular Sciences Laboratory, a national scientific user facility sponsored by the Department of Energy (DOE) Office of Biological and Environmental Research and located at Pacific Northwest National Laboratory, and used capabilities developed under efforts supported by the National Institute of General Medical Sciences Proteomics Research Resource (GM103493). PNNL is operated by Battelle Memorial Institute for the DOE under Contract DE-AC05-76RLO1830.

1. Mandl JN, et al. (2015) Reservoir host immune responses to emerging zoonotic viruses. *Cell* 160:20–35.
2. Kreuder Johnson C, et al. (2015) Spillover and pandemic properties of zoonotic viruses with high host plasticity. *Sci Rep* 5:14830.
3. Morse SS, et al. (2012) Prediction and prevention of the next pandemic zoonosis. *Lancet* 380:1956–1965.
4. Sawyer SL, Elde NC (2012) A cross-species view on viruses. *Curr Opin Virol* 2:561–568.
5. Menachery VD, Baric RS (2013) Bugs in the system. *Immunol Rev* 255:256–274.
6. Menachery VD, et al. (2014) Pathogenic influenza viruses and coronaviruses utilize similar and contrasting approaches to control interferon-stimulated gene responses. *MBio* 5:e01174-14.
7. Avgousti DC, et al. (2016) A core viral protein binds host nucleosomes to sequester immune danger signals. *Nature* 535:173–177.
8. Marazzi I, et al. (2012) Suppression of the antiviral response by an influenza histone mimic. *Nature* 483:428–433.
9. Lewandowska-Polak A, et al. (2015) Human parainfluenza virus type 3 (HPIV3) induces production of IFNγ and RANTES in human nasal epithelial cells (HNECs). *J Inflamm (Lond)* 12:16.
10. Pancham K, et al. (2015) Premature infants have impaired airway antiviral IFNγ responses to human metapneumovirus compared to respiratory syncytial virus. *Pediatr Res* 78:389–394.
11. Tenland E, et al. (2016) Innate immune responses after airway epithelial stimulation with Mycobacterium bovis Bacille-Calmette Guérin. *PLoS One* 11:e0164431.
12. Siezen CL, et al. (2009) Genetic susceptibility to respiratory syncytial virus bronchiolitis in preterm children is associated with airway remodeling genes and innate immune genes. *Pediatr Infect Dis J* 28:333–335.
13. Heller NM, et al. (2004) Interferon-gamma inhibits STAT6 signal transduction and gene expression in human airway epithelial cells. *Am J Respir Cell Mol Biol* 31:573–582.
14. Zissler UM, et al. (2016) Interleukin-4 and interferon-γ orchestrate an epithelial polarization in the airways. *Mucosal Immunol* 9:917–926.
15. Scobey T, et al. (2013) Reverse genetics with a full-length infectious cDNA of the Middle East respiratory syndrome coronavirus. *Proc Natl Acad Sci USA* 110:16157–16162.
16. Chakrabarti AK, et al. (2010) Host gene expression profiling in influenza A virus-infected lung epithelial (A549) cells: A comparative analysis between highly pathogenic and modified H5N1 viruses. *Virol J* 7:219.
17. Sarmento L, Afonso CL, Estevez C, Wasilenko J, Pantin-Jackwood M (2008) Differential host gene expression in cells infected with highly pathogenic H5N1 avian influenza viruses. *Vet Immunol Immunopathol* 125:291–302.
18. Wang Z, et al. (2014) Transcriptome analysis of the hippocampus in novel rat model of febrile seizures. *PLoS One* 9:e95237.
19. Guo Y, Korteweg C, McNutt MA, Gu J (2008) Pathogenetic mechanisms of severe acute respiratory syndrome. *Virus Res* 133:4–12.
20. Chu H, et al. (2014) Productive replication of Middle East respiratory syndrome coronavirus in monocyte-derived dendritic cells modulates innate immune response. *Virology* 454–455:197–205.
21. Chu H, et al. (2016) Middle East respiratory syndrome coronavirus efficiently infects human primary T lymphocytes and activates the extrinsic and intrinsic apoptosis pathways. *J Infect Dis* 213:904–914.
22. Tynell J, et al. (2016) Middle East respiratory syndrome coronavirus shows poor replication but significant induction of antiviral responses in human monocyte-derived macrophages and dendritic cells. *J Gen Virol* 97:344–355.
23. Summerfield A, McCullough KC (2009) Dendritic cells in innate and adaptive immune responses against influenza virus. *Viruses* 1:1022–1034.
24. Perrone LA, Plowden JK, García-Sastre A, Katz JM, Tumpey TM (2008) H5N1 and 1918 pandemic influenza virus infection results in early and excessive infiltration of macrophages and neutrophils in the lungs of mice. *PLoS Pathog* 4:e1000115.
25. Hatta Y, et al. (2010) Viral replication rate regulates clinical outcome and CD8 T cell responses during highly pathogenic H5N1 influenza virus infection in mice. *PLoS Pathog* 6:e1001139.
26. Rimmelzwaan GF, Katz JM (2013) Immune responses to infection with H5N1 influenza virus. *Virus Res* 178:44–52.
27. Arabi YM, et al. (2016) Feasibility of using convalescent plasma immunotherapy for MERS-CoV infection, Saudi Arabia. *Emerg Infect Dis* 22:1554–1561.
28. Alshukairi AN, et al. (2016) Antibody response and disease severity in healthcare worker MERS survivors. *Emerg Infect Dis* 22:1113–1115.
29. Smale ST, Tarakhovsky A, Natoli G (2014) Chromatin contributions to the regulation of innate immunity. *Annu Rev Immunol* 32:489–511.
30. Lieberman PM (2016) Epigenetics and genetics of viral latency. *Cell Host Microbe* 19:619–628.
31. Ferrari R, et al. (2014) Adenovirus small E1A employs the lysine acetylases p300/CBP and tumor suppressor Rb to repress select host genes and promote productive virus infection. *Cell Host Microbe* 16:663–676.
32. Seo YL, Heo S, Jang KL (2015) Hepatitis C virus core protein overcomes H2O2-induced apoptosis by downregulating p14 expression via DNA methylation. *J Gen Virol* 96:822–832.
33. Verweij MC, et al. (2015) Viral inhibition of the transporter associated with antigen processing (TAP): A striking example of functional convergent evolution. *PLoS Pathog* 11:e1004743.
34. Aevermann BD, et al. (2014) A comprehensive collection of systems biology data characterizing the host response to viral infection. *Sci Data* 1:140033.
35. McDermott JE, et al. (2016) The effect of inhibition of PP1 and TNFα signaling on pathogenesis of SARS coronavirus. *BMC Syst Biol* 10:93.

36. Gralinski LE, et al. (2013) Mechanisms of severe acute respiratory syndrome coronavirus-induced acute lung injury. *MBio* 4:e00271-13.
37. Sims AC, et al. (2013) Release of severe acute respiratory syndrome coronavirus nuclear import block enhances host transcription in human lung cells. *J Virol* 87: 3885–3902.
38. Josset L, et al. (2013) Cell host response to infection with novel human coronavirus EMC predicts potential antivirals and important differences with SARS coronavirus. *MBio* 4:e00165–e13.
39. Gibbs DL, et al. (2013) Protein co-expression network analysis (ProCoNA). *J Clin Bioinforma* 3:11.
40. Li C, et al. (2011) Host regulatory network response to infection with highly pathogenic H5N1 avian influenza virus. *J Virol* 85:10955–10967.
41. Yount B, et al. (2003) Reverse genetics with a full-length infectious cDNA of severe acute respiratory syndrome coronavirus. *Proc Natl Acad Sci USA* 100:12995–13000.
42. Neumann G, et al. (1999) Generation of influenza A viruses entirely from cloned cDNAs. *Proc Natl Acad Sci USA* 96:9345–9350.
43. Webb-Robertson BJ, et al. (2010) Combined statistical analyses of peptide intensities and peptide occurrences improves identification of significant peptides from MS-based proteomics data. *J Proteome Res* 9:5748–5756.
44. Matzke MM, et al. (2011) Improved quality control processing of peptide-centric LC-MS proteomics data. *Bioinformatics* 27:2866–2872.
45. Webb-Robertson BJ, Matzke MM, Jacobs JM, Pounds JG, Waters KM (2011) A statistical selection strategy for normalization procedures in LC-MS proteomics experiments through dataset-dependent ranking of normalization scaling factors. *Proteomics* 11: 4736–4741.
46. Matzke MM, et al. (2013) A comparative analysis of computational approaches to relative protein quantification using peptide peak intensities in label-free LC-MS proteomics experiments. *Proteomics* 13:493–503.